Ultrashort pulsed laser ablation of zirconia-alumina composites for implant applications

Jide Han[1], Olivier Malek[2], Jozef Vleugels[3], Annabel Braem[3], Sylvie Castagne[1, *]

[1] KU Leuven, Department of Mechanical Engineering and Flanders Make@KU Leuven-MaPS, 3001 Leuven, Belgium

[2] Sirris Precision Manufacturing, 3590 Diepenbeek, Belgium

[3] KU Leuven, Department of Materials Engineering, 3001 Leuven, Belgium

* sylvie.castagne@kuleuven.be

Abstract

Laser texturing of zirconia-alumina ceramics is a promising surface modification method for many applications, such as enhancing osseointegration of alumina toughened zirconia (ATZ) dental implants or improving friction behavior of zirconia toughened alumina (ZTA) hip replacement bearing components. The common problems in laser texturing of ATZ/ZTA ceramics are thermal cracking, low material removal rate (MRR), and laser-induced phase transformation (LIPT). Furthermore, the compositional variation of those ceramics will complicate these problems. In order to improve the manufacturing processability, ultrashort pulsed laser ablation behavior of ATZ/ZTA composites was investigated in this research. Single phase zirconia and alumina were found to have smaller MRRs than their composites, and this behavior was negatively correlated to the materials single-pulse laser ablation threshold. However, under multi-pulse laser irradiation, the ablation thresholds of all materials saturated to the same level, indicating that single phase materials were more sensitive to the incubation effect than their composites. This led to the MRRs of the single phase materials being reduced at larger scan speeds, while the MRRs of their composites remained independent of scan speed. It was also shown that single phase materials were less susceptible to thermal cracking than their composites under excessive heat accumulation. These results suggest that a lower scan speed is preferred for single phase materials in order to achieve a larger MRR, while a higher scan speed is beneficial for the composites for suppressing thermal cracking without compromising ablation efficiency. In addition, no LIPT was detected for zirconia dominated materials after laser ablation.

Keywords

Femtosecond laser; Laser ablation threshold; Alumina-zirconia composite; Incubation effect; Material removal rate

1. Introduction

Zirconia based ceramics, including yttria-stabilized tetragonal zirconia polycrystals (Y-TZP) and alumina-zirconia composites, i.e. alumina toughened zirconia (ATZ) and zirconia toughened alumina (ZTA), are promising materials for implant applications, including dental and hip joint implants, due to their excellent properties, such as biocompatibility, high fracture toughness, high strength and wear resistance, as well as good esthetic properties (Gautam et al., 2016). Y-TZP, typically the 3Y-TZP variant which contains 3 mol% Y_2O_3, exhibits the best mechanical properties in terms of fracture toughness and strength among all oxide ceramics (Wei and Gremillard, 2018). This is attributed to the stress induced tetragonal-to-monoclinic phase transformation around a possible crack tip which induces a compressive stress field due to the volume expansion thus inhibiting crack propagation (Piconi and Maccauro, 1999). This transformation, however, can also occur in humid environment at relatively low temperatures, which is exactly the case in the body environment, leading to degradation of both mechanical and esthetic properties (Ramesh et al., 2018). Alumina-zirconia composites were developed to overcome this intrinsic weakness of Y-TZP, but with a compromise on the fracture toughness as a higher fraction of alumina leads to a better hydrothermal ageing resistance, but a lower fracture toughness. Boniecki et al. (2020) showed that the fracture toughness of alumina-zirconia composites decreased while the hardness increased with increasing alumina content. This behavior makes the alumina-zirconia composite with a lower content of alumina more suitable for making dental implants, where a high fracture toughness is required, while the composites with a higher content of alumina more suitable for making hip joint implants, where high wear resistance is of vital importance.

The long-term stability of implants is strongly dependent on the mechanical properties and hydrothermal ageing resistance of the alumina-zirconia composites of which they are made. Yet, their interaction with the human body environment is also an important factor which can be strongly influenced by their surface condition (Schunemann et al., 2019). For dental implants, the surface of the endosseous part is intentionally roughened in order to improve osseointegration. There are many methods to modify the surface of dental implants, e.g. machining, sand blasting, acid etching, and laser processing (Schunemann et al., 2019). Among these methods, a big advantage of laser processing is that it is possible to obtain predesigned regular micro-textures and this selectively on different locations on the implant surface. This allows to fine-tune different parts of the implant for an enhanced functionality, such as regulating bone cell behavior at the endosseous level of a dental implant to increase the osseointegration process (Delgado-Ruiz et al., 2015) or preventing bacterial adhesion at the abutment level to reduce peri-implant infections (Lu et al., 2020). However, there are also limitations to laser processing, including a low material removal rate (MRR), unwanted heat affected layer formation, the generation of thermal cracks (Roitero et al., 2017), and a laser-induced phase transformation (Roitero et al., 2018). A comprehensive review about laser texturing of zirconia-based ceramics for dental applications can be found in a recent paper (Han et al., 2021b).

Since laser machining is the result of laser-material interactions, both laser parameters and material properties can influence the laser machining outcome. Li et al. (2016) investigated the influence of different laser parameters, including laser fluence, number of laser pulses, and scan speed on material removal behavior of 3Y-TZP. Laser machining process optimization based on design of experiments and multi-objective genetic algorithm was conducted by Abdo et al. (2018) for minimizing ablation dimensional error and heat-affected zone in laser processed 3Y-TZP. Available research in literature mainly focused on the influence of the laser processing parameters on the machining performance of zirconia based ceramics, and there is still a lack of understanding on how the composition of an alumina-zirconia composite affects the laser micromachining performance. Therefore, in this research, the influence of the material composition on femtosecond laser processing of alumina-zirconia composites was investigated by varying the alumina content from 0 to 100 wt%. The laser ablation thresholds and incubation effect for materials with increasing alumina content were analyzed. The influence of experimental parameters as well as material composition on the MRR was determined experimentally. This research will not only expand the knowledge on fundamental mechanisms occurring during laser processing of alumina-zirconia composites, but will also serve as a useful reference for the design of zirconia based ceramics for implant applications, taking into account the laser machinability aspects in addition to fracture toughness and thermal aging resistance considerations.

2. Materials and methods

2.1 Ceramic preparation

A set of six grades of alumina-zirconia composites with varying alumina contents was prepared by pressureless sintering. Firstly, six powder mixtures with different proportions of 3 mol% Y_2O_3-stabilized ZrO_2 (TZ-3Y, Tosoh, 50 nm) were wet mixed with Al_2O_3 (TM-DAR, Taimicron, 0.22 μm) in ethanol for 24 h on a WAB Turbula multi-directional mixer with 5 mm ZrO_2 milling media. The proportions of Al_2O_3 increased from 0 to 100 wt% with an interval of 20 wt% as indicated in Table

1, showing the composition of the six material grades. The ethanol was removed from the wet mixed powder on a rotating evaporator and oven-dried overnight at 85°C. The dried powder was uniaxially pressed (25 kN, 1 min) and subsequently cold isostatically pressed (300 MPa, 1 min) to form a green powder compact that was sintered at 1500°C in air for 2 h. The heating and cooling rate was set at 10°C/min from 40–1000°C and 5°C/min from 1000–1500°C. The sintered ceramics were polished with diamond paste to obtain a surface roughness below 10 nm before laser processing.

Table 1. Composition of the alumina-zirconia composites investigated by femtosecond laser processing.

Materials	ZrO_2 (wt%)	Y_2O_3 (wt%)	Al_2O_3 (wt%)
3Y-TZP	94.6	5.4	0
20%-Al_2O_3	75.7	4.3	20
40%-Al_2O_3	56.8	3.2	40
60%-Al_2O_3	37.8	2.2	60
80%-Al_2O_3	18.9	1.1	80
Al_2O_3	0	0	100

2.2 Femtosecond laser processing

The ceramics were laser processed by a femtosecond laser (SATSUMA, Amplitude Systems) with a Gaussian beam profile. The pulse width is 250 fs, and the wavelength is 1030 nm. The maximum average power of the laser source is 10 W, and the maximum pulse energy is 20 μJ. The focal length of the focus lens is 100 mm. The total optical loss of the equipment is 21.5%. The maximum pulse repetition rate (PRR) is 500 kHz. Stationary crater machining with single and multi-pulse and groove machining experiments were performed in normal atmospheric conditions. The detailed experimental parameters are listed in Table 2. The laser machined ceramics were examined by scanning electron microscopy (SEM, XL30 FEG, FEI) for morphology examination and confocal microscopy (S-neox, Sensofar) for topography measurement. Micro-Raman spectroscopy (SENTERRA, BrukerOptik, Ettlingen, Germany) was used to examine the potential phase transformation in laser grooved areas.

Table 2. Experimental parameters for crater and groove machining

Experiments	Crater machining	Groove machining
Pulse energy (μJ)	4.4, 6.0, 7.7, 9.4, 11.0, 12.4, 13.7, 14.6, 15.4	6.0, 7.7, 9.4, 11.0, 12.4, 13.7, 14.6, 15.4
Number of pulses	1, 2, 5, 10, 20, 100	4, 2.7, 2, 1.6[a]
Scan speed (mm/s)	-	1000, 1500, 2000, 2500
PRR (kHz)	100	500

[a]The values are equivalent number of pulses

3. Results and discussion

3.1 Characterization

The microstructure of the bulk materials, as observed by SEM on polished surfaces after thermal etching at 1300°C for 20 minutes, are shown in Fig. 1. The two phases of the alumina-zirconia composites can be clearly distinguished. The bright color phase being zirconia and the dark color phase being alumina. The two constituent phases of the composite ceramics were uniformly distributed. The grain sizes of the phases in the ceramics were measured (Fig. 2) by the linear intercept method with a multiplication factor of 1.56 adopted for the 2D to 3D conversion

(Mendelson, 1969). In general, the grain sizes of both zirconia and alumina decreased with increasing secondary phase content in the composites. This is because of the Zener pinning effect of the secondary phase on the grain boundaries during sintering. The density of the samples was measured in triplicate by the water displacement method. The results are shown in Fig. 3 (a). The density decreased with increasing alumina content. This is as expected since the density of pure alumina (3.98 g/cm^3) is lower than that of 3Y-TZP (6.1 g/cm^3). The relative density was calculated as the measured density divided by the theoretical one which is also shown in this figure. Almost fully dense material was obtained for all the combinations with the lowest relative density being 98.4% for the composite with 20 wt% of alumina. The Vickers hardness was measured with an indentation load of 1 kg during 10 s. Five indentations were averaged for each material. As shown in Fig. 3 (b), the hardness increased with increasing alumina content, which is in line with the higher intrinsic hardness of pure alumina as compared to 3Y-TZP.

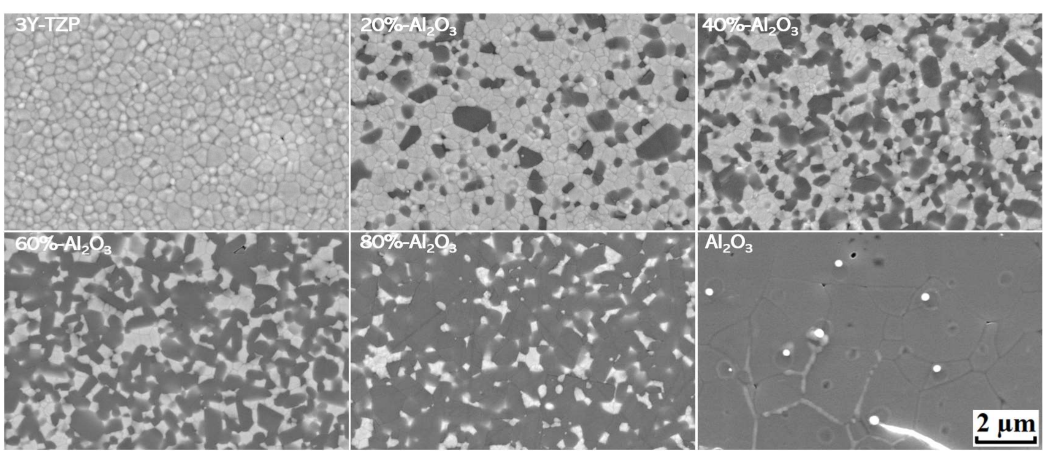

Fig. 1. Representative SEM images of the alumina-zirconia composites after thermal etching with increasing alumina content from 0 to 100 wt% (zirconia is the bright

phase, alumina is the dark one).

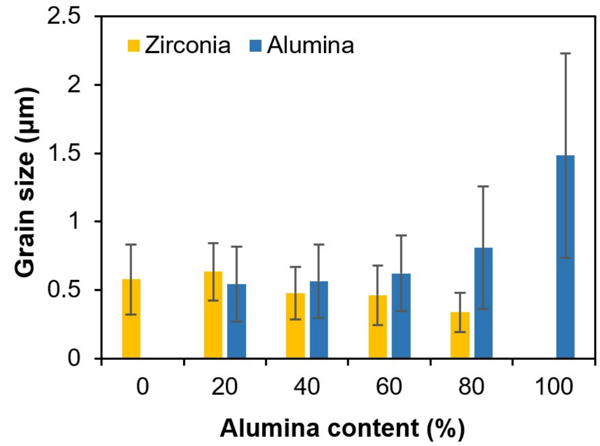

Fig. 2. Grain sizes of the Al_2O_3 and ZrO_2 phases in the ceramics as a function of the overall alumina content.

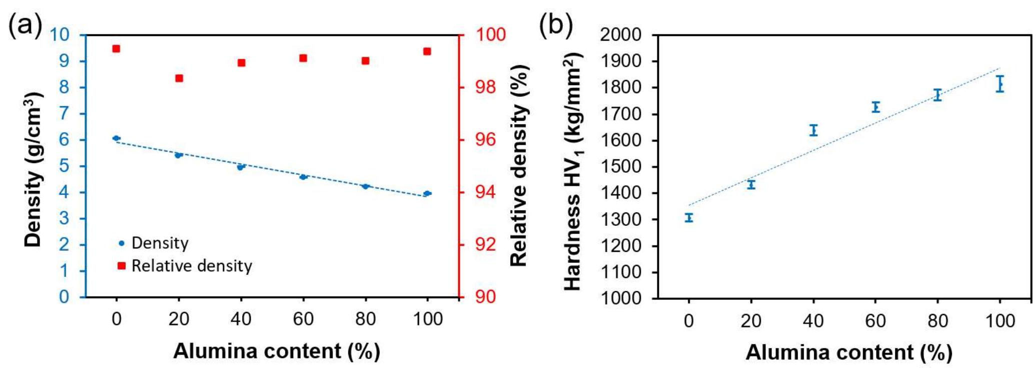

Fig. 3. (a) Ceramic density and relative density as a function of the alumina content; (b) Vickers hardness as a function of the alumina content.

The procedure for the determination of the MRR is illustrated in Fig. 4. Firstly, the average groove profile over a distance of 25 μm was extracted from the confocal microscopy measurement results. Secondly, the area of the extracted profile was calculated by the data analysis software of the confocal microscope. The MRR can be determined by multiplying the profile area by the scan speed. The MRR was averaged over three measurements for each experimental condition.

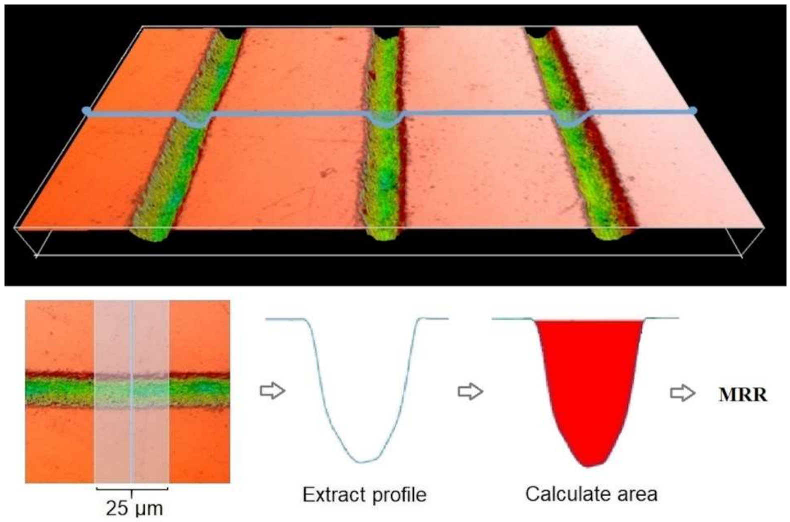

Fig. 4. Schematic diagram of MRR determination procedure. Firstly, the average groove profile over a distance of 25 μm was extracted from the confocal microscopy measurement result. Secondly, the area of the extracted profile was calculated by the data analysis software of the confocal microscopy. The MRR can be determined by multiplying the profile area by the scan speed.

3.2 Laser ablation thresholds and incubation effect

The single and multi-pulse laser ablation thresholds (F_{th}) were calculated using the D^2 method where $D^2 = 2\omega_0^2 ln\,(F_0/F_{th})$ (Liu, 1982), with D and ω_0 the diameter of the laser ablation crater and laser beam radius at $1/e^2$ of the peak fluence, respectively. The laser peak fluence $F_0 = 2E_0/(\pi\omega_0^2)$. The beam diameter was calculated to be 16 μm in this experiment. Fig. 5 (a) shows the squared diameter of the single pulse ablation craters as a function of the logarithm of the laser fluence for the materials with increasing alumina content. The single pulse laser ablation threshold of the materials is plotted in Fig. 5 (b). For pure alumina, due to the high ablation threshold as well as the limitation of the experimental setup in terms of maximum pulse energy, there were not enough data to plot the fitting line in Fig. 5 (a). The ablation threshold of alumina was calculated assuming that the slope of the fitting line of alumina is the same as for zirconia. This is reasonable since the slope of the fitting line indicates the diameter of the laser focal spot which should be the same in processing different materials. Fig. 5 (b) shows that the ablation thresholds of the alumina-zirconia composites are smaller than those of both pure alumina and 3Y-TZP, which implies that for the single pulse laser ablation case, the composite materials could be more easily ablated as compared to the base materials they are made of.

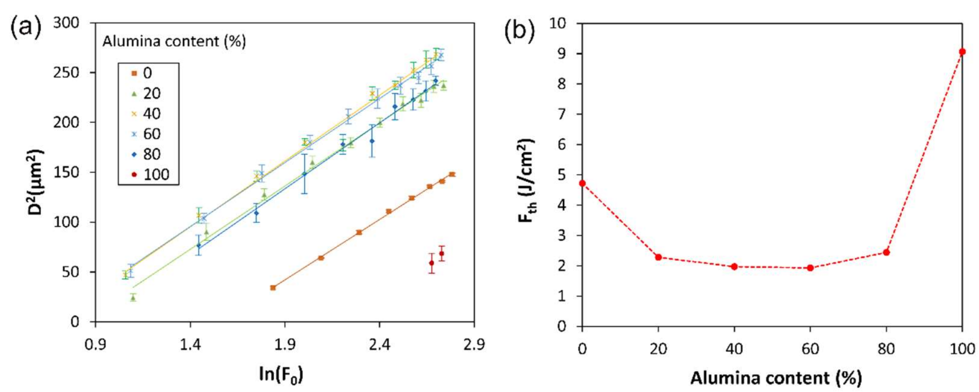

Fig. 5. (a) Squared diameter of single pulse ablation craters as a function of the logarithm of the laser fluence (J/cm^2) for the alumina-zirconia composites; (b) the single pulse ablation threshold for different materials as a function of alumina content.

Although the shape of the curve in Fig. 5 (b) looks similar to the shape of the eutectic alumina-zirconia phase diagram, since the melting points of alumina-zirconia composites exhibit a similar trend than their ablation thresholds, the melting point of zirconia (2715°C) is much higher than that of alumina (2072°C), while the laser ablation threshold of zirconia is smaller than that of alumina. This indicates that the laser ablation threshold of a ceramic material is not or not solely determined by its melting point in femtosecond laser processing condition.

When the band gap of a ceramic material is larger than the energy of a single photon, the laser absorption is a highly non-linear process, the laser absorption mechanisms including avalanche ionization, multiphoton absorption and tunneling ionization (Shugaev et al., 2016). It is the band gap of the ceramic material that plays a dominant role in the determination of laser energy absorption and therefore its ablation threshold. Since the band gap of zirconia (5.8 eV) is smaller than that of alumina (8.8 eV) , the ablation threshold of zirconia is also smaller than for alumina (Robertson, 2004). As the alumina-zirconia composites are composed of two phases with submicrometer grain sizes, it is meaningless to describe their band gaps with a single value. Therefore, it is not possible to directly link their ablation thresholds to the band gap. The laser ablation threshold of a material is also influenced by its containing defects since the presence of defects can enhance the absorption of laser energy. As a result, the laser ablation threshold will reduce with increasing defect density (Armbruster et al., 2018). The composite materials normally have a smaller grain size and a higher quantity of alumina-zirconia grain boundaries. Therefore, there is a high possibility that these grain boundaries could contain more defects compared to the zirconia-zirconia and alumina-alumina grain boundaries due to the crystal lattice mismatch between zirconia and alumina. This could be a possible reason for the reduction of laser ablation thresholds for the composite materials.

For multi-pulse laser ablation, the laser ablation thresholds will be smaller than those of single pulse laser ablation due to the incubation effect. The relationship can be described by $F_{th}(N) = F_{th}(1)N^{S-1}$, where N is the number of pulses, S is the incubation coefficient (Jee et al., 1988). This incubation model was initially proposed for nanosecond laser irradiation of metals. The cumulative effect of laser pulses on the change of laser damage threshold was explained by the storage cycle of laser-induced thermal stress-strain energy, in analogy to that of the mechanical fatigue damage behavior of metals. The model was then also shown to be applicable for femtosecond laser irradiation of dielectrics, although the thermal stress-strain energy storage explanation is not valid for dielectrics anymore (Bonse et al., 2000). The laser ablation thresholds of the alumina-zirconia composite materials for a varying number of laser pulses is shown in Fig. 6 (a), while Fig. 6 (b) shows the corresponding incubation coefficients. A smaller incubation coefficient implies that the material will be more sensitive to the accumulation effect of the laser pulses. Fig. 6 (a) shows that the differences in laser ablation threshold for different materials gradually reduced with increasing number of pulses. This resulted in smaller incubation coefficients for the phase pure materials than for their composites. Moreover, the ablation threshold tends to saturate at a certain value when the number of irradiated laser pulses is large enough, and the differences in ablation threshold between different materials gradually vanish. However, according to the above equation, the ablation threshold will decrease to zero when the applied number of laser pulses is infinite. This is not in agreement with the experimental results, and it is the main limitation of this incubation model. Ashkenasi et al. (1999) proposed an improved model for femtosecond laser irradiation of dielectrics to account for the saturation effect. The model is based on the assumption of the occurrence of laser-induced defects accumulation and is written as: $F_{th}(N) = F_{th}(\infty) + [F_{th}(1) - F_{th}(\infty)]\exp[-k(N - 1)]$, where k is an empirical parameter that indicates the strength of defects accumulation. $F_{th}(\infty)$ is the saturation fluence which is the minimum fluence required to induce laser damage with infinite number of laser pulses. Di Niso et al. (2014) proposed a similar model by just adding a constant term to the original incubation model proposed by Jee et al. (1988). The model can then be written as: $F_{th}(N) = F_{th}(\infty) + F_{th}(1)N^{S^*-1}$, where S^* is the modified incubation coefficient (Di Niso et al., 2014). The introduction of the saturation fluence term ensures that the predicted laser damage threshold is consistent with experimental observations and will converge to a finite value when the applied number of laser pulses is infinite. The laser damage threshold at infinite number of laser pulses irradiation, or the saturation fluence, is a critical parameter for an optical component since it determines the maximum allowable energy density that it can withstand. However, in a laser machining process, the workpiece material at a specific location is normally subject to a very limited number of laser pulses irradiation. Therefore, the model proposed by Jee et al. (1988) is sufficient for the prediction of the multi-pulse laser ablation threshold in this situation. Also because of its simplicity, this model was most widely used in academia and industry (Heisterkamp et al., 2016).

A larger incubation coefficient *S* means that the material is less sensitive to the incubation effect, i.e. the accumulation of laser pulses at the same location will not reduce the ablation threshold notably. Therefore, each pulse will remove approximately the same amount of material. However, for the single phase zirconia and alumina, the incubation coefficients are smaller than for their composites, which means they are more sensitive to the accumulation effect of laser pulses. More laser pulses accumulated at the same location will notably reduce the ablation threshold. As a consequence, the subsequent laser pulses will be able to remove larger amounts of material than previous pulses. This is the reason why the MRRs of the single phase materials show different trends when compared to the MRRs of their composites when changing scan speed, as will be shown in section 3.4.2 below.

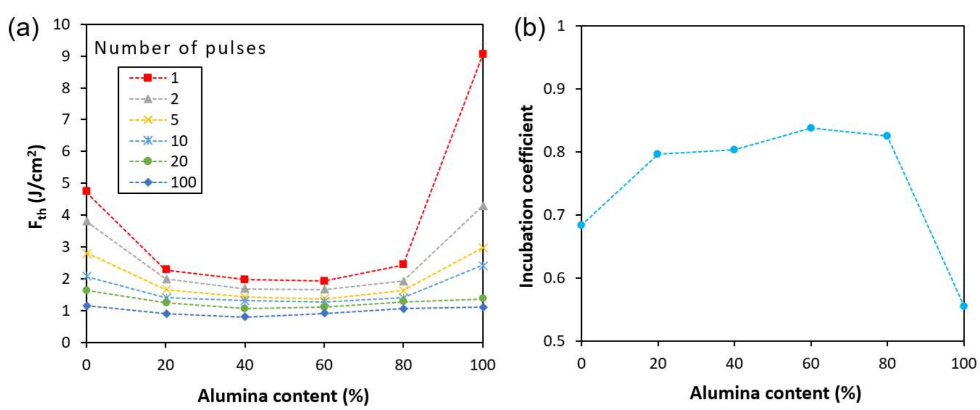

Fig. 6. (a) Laser ablation thresholds under varying number of laser pulses as a function of alumina content; (b) incubation coefficients as a function of alumina content.

3.3 Laser ablated crater morphology and thermal cracks

The morphology of single and multi-pulse laser ablated areas was examined by SEM. Representative images of single and 100-pulse laser ablation samples are shown in Fig. 7. For the single pulse laser ablation, the ablated areas of the composite materials were larger than for the phase pure materials, which signifies that the composite materials have smaller ablation thresholds than the phase pure materials. Moreover, the edges of the ablated circles of the phase pure materials, especially the zirconia sample, were generally smoother than that of the composite materials. This is because the composite materials are composed of two phases having different ablation thresholds that makes them inhomogeneous at the microscale; therefore the ablation behavior at the edge area was rather stochastic.

For the 100-pulse laser ablation results (Fig. 7 (b)), besides the much larger ablation depths, another noticeable phenomenon was that cracks were more easily formed on the sidewall of the holes of the composite materials than on the phase pure materials. This could be attributed to the smaller laser ablation thresholds of the composite materials. Since less energy was required to remove the same amount of composite material than phase pure material, the more excessive energy input in the composite materials under the same laser parameter conditions may cause some adverse effects such as the formation of thermal cracks.

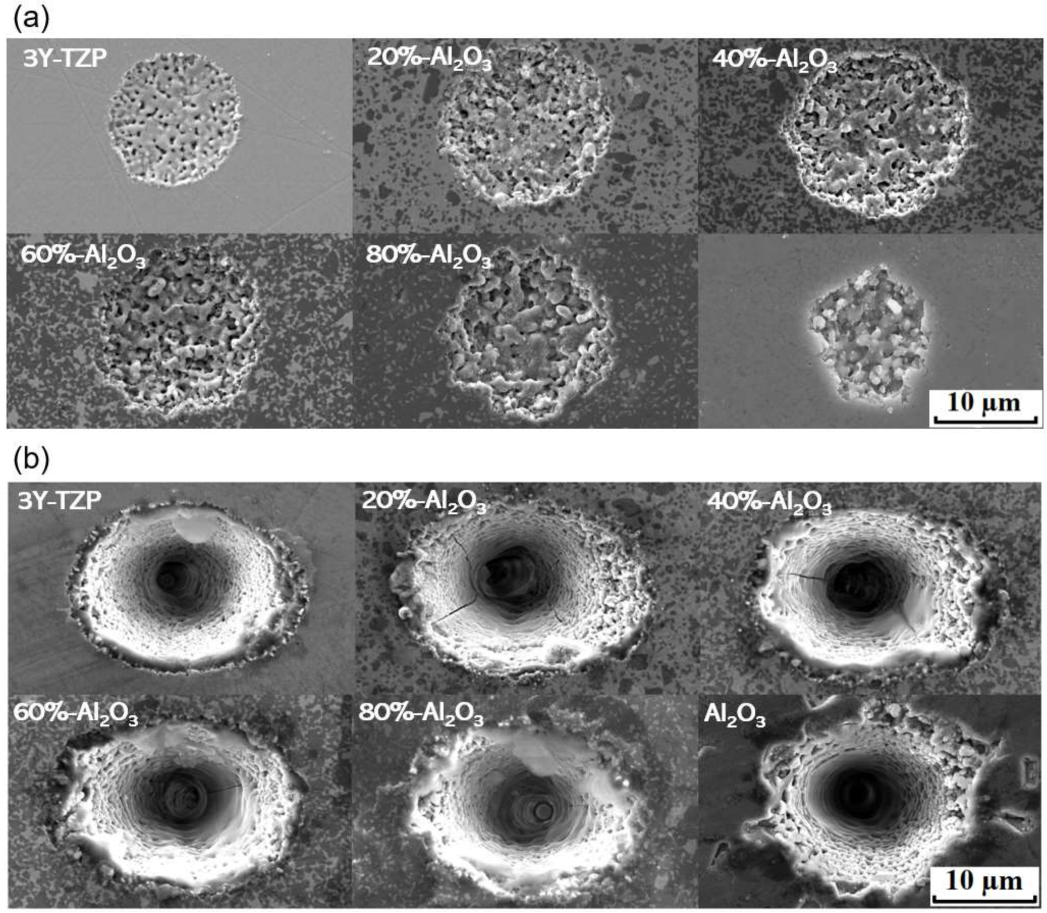

Fig. 7. Representative SEM images of the alumina-zirconia composites with increasing alumina content after laser ablation with (a) 1 pulse; (b) 100 pulses. The laser pulse energy was 15.4 μJ.

3.4 Laser grooving and MRR

Laser grooving was conducted to investigate the influence of laser pulse energy, scan speed, and material composition on MRR. Representative SEM images of the laser grooving experiment are shown in Fig. 8. Due to the smaller ablation thresholds, the groove widths on the composite materials were larger than on the phase pure materials. Besides, the groove edge on alumina was much rougher than on the other materials, while zirconia showed the best groove quality. The groove profiles were measured by confocal microscopy. The procedure for the determination of the MRR is illustrated in Fig. 4.

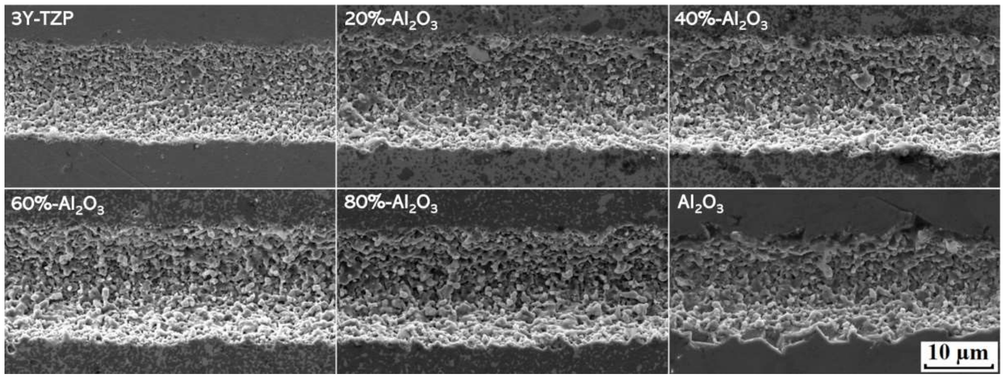

Fig. 8. Representative SEM images of the alumina-zirconia composites with increasing alumina content after laser grooving experiments. Laser pulse energy:15.4 μJ; scan speed: 1000 mm/s; PRR: 500 kHz.

3.4.1 Influence of laser pulse energy

For pulsed laser micromachining, the MRR is influenced by experimental parameters, mainly laser power and scan speed, as well as material properties. When the PRR is fixed, the average laser power is proportional to the pulse energy, i.e. laser power = PRR × pulse energy. In this laser grooving experiment, the PRR was set to 500 kHz, which is the maximum value of the equipment adopted, for maximizing the MRR. Fig. 9 shows the representative groove profiles of the 3Y-TZP material after laser grooving with increasing pulse energies. The ablation depth and width increased with increasing laser pulse energy as expected. For the other materials with varying alumina content, the trends are the same although the absolute values of the ablation depth and width are different.

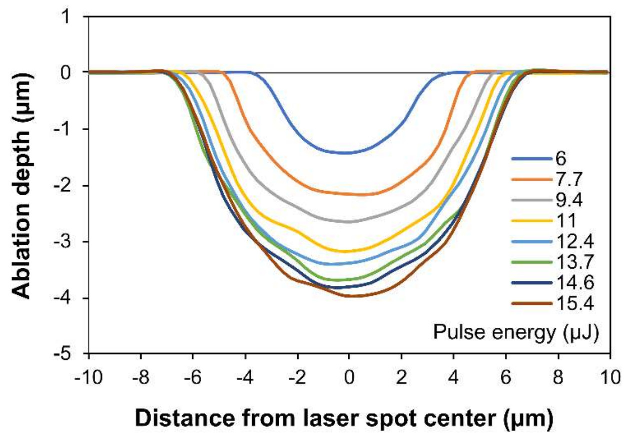

Fig. 9. The influence of laser pulse energy on ablation groove profiles of 3Y-TZP (PRR: 500 kHz, scan speed: 1000 mm/s).

The MRR for varying composite as a function of laser pulse energy is plotted in Fig. 10 (a). The MRR is nearly proportional to the laser pulse energy for all materials. However, the slopes of the fitting lines are varying for the different materials. Generally, a higher alumina content of the material corresponds to a larger fitting line slope as shown in Fig. 10 (b). This means that when increasing laser power, the MRR of a material with a higher alumina content increased faster than that of a material with a lower alumina content. This is because at a higher laser power, the thermal effect becomes more prominent due to a larger amount of laser energy being absorbed by the materials. The melting and vaporization temperatures of alumina are 2072°C and 2977°C, which are much lower than that of zirconia which are 2715°C and 4300°C. This means that removing the same amount of alumina material by thermal effect will consume less energy than for zirconia even though alumina has a slightly larger volumetric heat capacity than zirconia. Therefore, the MRR of materials with higher alumina contents increased faster than that of materials with lower alumina contents. For zirconia, it is also possible to fit the data with a logarithmic function as shown in Fig. 10 (a) by the dotted line, and it gives a better fitting than a linear function. Since the curvature of the logarithmic fitting line is small, a linear fitting is still a good approximation in this case.

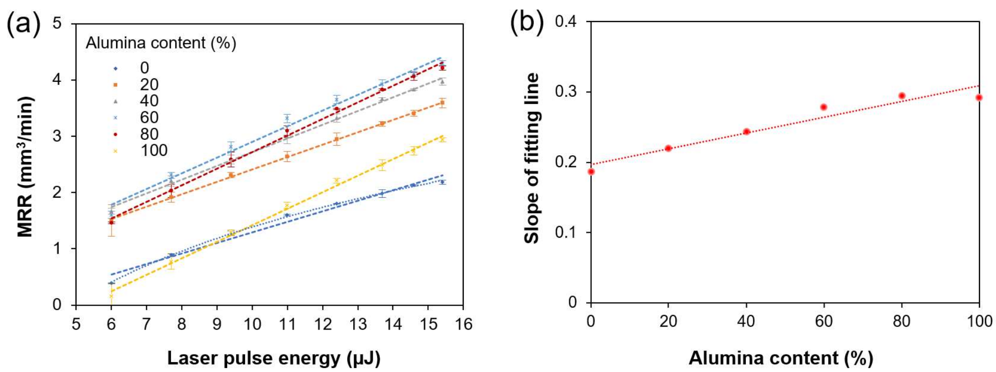

Fig. 10. (a) MRR as a function of laser pulse energy for the alumina-zirconia composites with increasing alumina contents (PRR: 500 kHz, scan speed: 1000 mm/s); (b) the slope of the fitting line in (a) as a function of alumina content.

3.4.2 Influence of scan speed

Scan speed can influence the laser groove profile by affecting the total amount of energy deposition at each position. A larger scan speed will lead to a smaller groove depth. While the MRR is the product of groove area and scan speed; the influence of scan speed on MRR is not that obvious and needs to be investigated experimentally. Fig. 11 shows the MRR as a function of scan speed for materials with increasing alumina content. The scan speed ranged from 1000 to 2500 mm/s with an interval of 500 mm/s. At scan speeds larger than 1500 mm/s, there was no regular groove generated on the alumina surface; therefore, no data was presented in this figure. The experimental results showed that the MRR decreased with increasing scan speed for zirconia and alumina; while the MRR was nearly independent of the scan speed for the composites. This behavior is related to the incubation effect of the materials. For zirconia and alumina, the laser ablation thresholds reduced more significantly than for the composite materials when increasing laser pulses. This indicates that for zirconia and alumina, the amount of material removed by a unit laser energy when the energy is supplied through a lower number of laser pulses irradiation is smaller than when this energy is supplied through a higher number of laser pulses irradiation. However, for the composite materials, each laser pulse will remove almost the same amount of material in single or multi-pulse laser ablation. For example, if one laser pulse will remove one unit amount of material during single pulse laser ablation of zirconia and alumina, a two-pulse laser ablation at the same position will remove more than two unit amounts of material. Since changing the scan speed is almost equivalent to changing the number of pulses at each position in laser grooving, with a lower scan speed, the total amount of material removed per unit of time (the MRR), is larger than that with a higher scan speed. While for the composite materials, two-pulse laser ablation will remove two unit amounts of material. As a result, the amount of material removal is only determined by the total number of laser pulses and the MRR is independent of the laser scan speed.

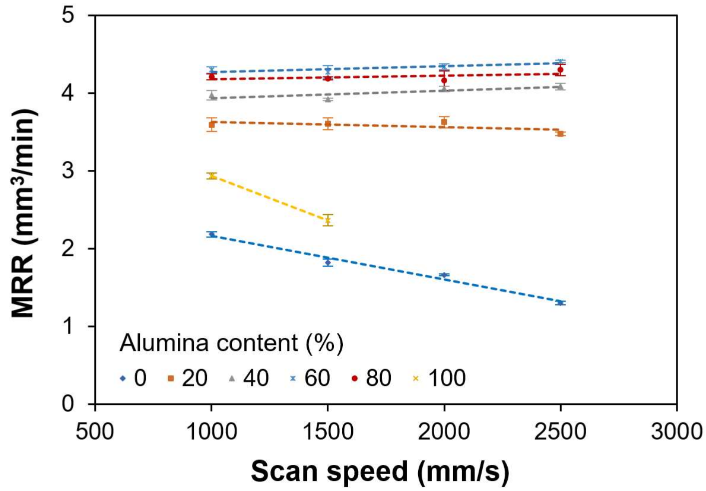

Fig. 11. MRR as a function of scan speed for the alumina-zirconia composites with increasing alumina contents (Laser pulse energy:15.4 μJ, PRR: 500 kHz).

The groove profiles for 3Y-TZP and 60%-Al_2O_3 under increasing laser scan speeds are plotted in Fig. 12. Besides the larger groove depths of 60%-Al_2O_3 compared to 3Y-TZP under the same scan speeds, the groove width of 3Y-TZP decreased with increasing scan speed, while there was almost no change in case of 60%-Al_2O_3. This is also because the incubation effect for 3Y-TZP is more significant than for Al_2O_3. The incubation coefficient calculated in the previous section can be seen as a parameter that quantifies the change in width under different scan speeds. The smaller the incubation coefficient, the more the groove width will change.

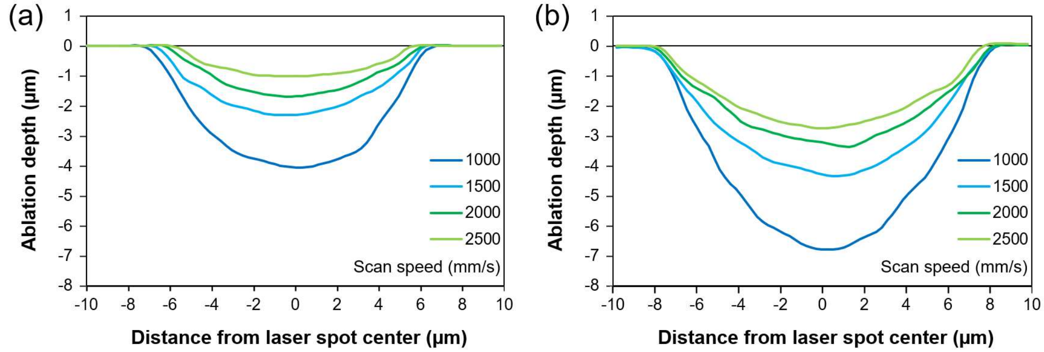

Fig. 12. Groove profiles of (a) 3Y-TZP and (b) 60%-Al_2O_3 under varying laser scan speeds (Laser pulse energy:15.4 μJ, PRR: 500 kHz).

3.4.3 Influence of composition

In section 3.1, it has been shown that the composite materials have smaller ablation thresholds than the phase pure materials. Since the laser ablation threshold indicates how difficult a material can be ablated by laser energy, it should have a correlation with the MRR. Fig. 13 (a) compares the laser ablated groove profiles of the materials with increasing alumina content under the same experimental parameters. It shows that besides the experimental parameters, the material composition also has a significant influence on the laser ablation behavior. Fig. 13 (b) shows the MRR as a function of alumina content under three typical pulse energy conditions. Under all these conditions, the MRR of the composite materials was larger than those of the phase pure materials. When the pulse energy was low, the MRR of zirconia was larger than for alumina, while with increasing pulse energy, the MRR of alumina increased faster than that of zirconia, and at the highest pulse energy, the MRR of zirconia became smaller than for alumina. A tentative explanation for this behavior was provided in section 3.4.1. Since all ceramics were almost fully dense, the difference in MRR between the various composites studied cannot be attributed to residual porosity. The grain size may have an influence on the material removal behavior of a specific material, but it cannot directly explain the difference in MRR between different materials. Further research is still required to get a fundamental understanding of the phenomena explaining the relationship between MRR and composition.

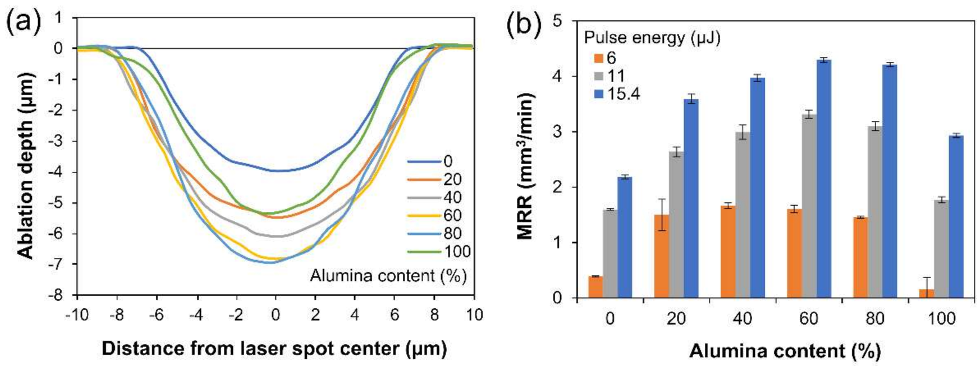

Fig. 13. (a) Laser ablated groove profiles of the alumina-zirconia composites with increasing alumina content (laser pulse energy:15.4 μJ, PRR: 500 kHz, scan speed: 1000 mm/s); (b) MRR as a function of alumina content (PRR: 500 kHz, scan speed: 1000 mm/s).

3.4.4 Phase transformation and composition changes

A major concern when using zirconia in dental applications is its low temperature degradation behavior (Lughi and Sergo, 2010). The metastable tetragonal phase of zirconia has a tendency of transforming to the monoclinic phase in the presence of water or humidity, which will result in a deterioration of the mechanical strength of the material. This is mainly a concern for higher zirconia content ceramics, such as 3Y-TZP and ATZ with 20 wt% of alumina (20%-ATZ). This tetragonal to monoclinic phase transformation could also happen during the laser micromachining process, although most literature studies indicated that laser induced phase transformation (LIPT) is negligible for short pulse laser processing (Han et al., 2021b). In this research, the LIPT of 3Y-TZP and 20%-ATZ was measured by confocal micro-Raman spectroscopy with a laser wavelength of 532 nm and an objective of 20×. Representative measurement results are shown in Fig. 14. No intensity change of the monolithic doublet was observed between polished and laser grooved areas, indicating there was no LIPT, which is in accordance with most of the research studies in literature (Han et al., 2021b). In a recent research paper by the authors, a selective phase removal was observed for the alumina-zirconia composites, which indicated that the zirconia phase is easier to be removed by femtosecond laser than the alumina phase (Han et al., 2021a). In this research, it was also observed that the zirconia content of the laser grooved area of all the composites was slightly lowered compared to the original polished surface as shown in Fig. 15. In contrast, there was no regular change of the alumina element content being observed for the composites.

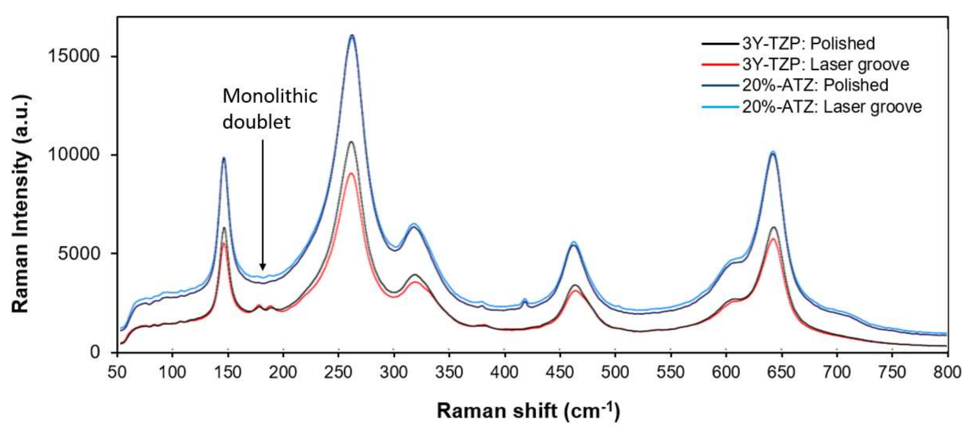

Fig. 14. Micro-Raman spectra of polished and laser grooved area of 3Y-TZP and 20%-ATZ. The laser parameters for the measured grooves were: PRR of 500 kHz, scan speed of 1000 mm/s, and laser pulse energy of 6 μJ. The measurement was performed on 3 locations for each condition. One representative spectrum for each condition is shown in the figure.

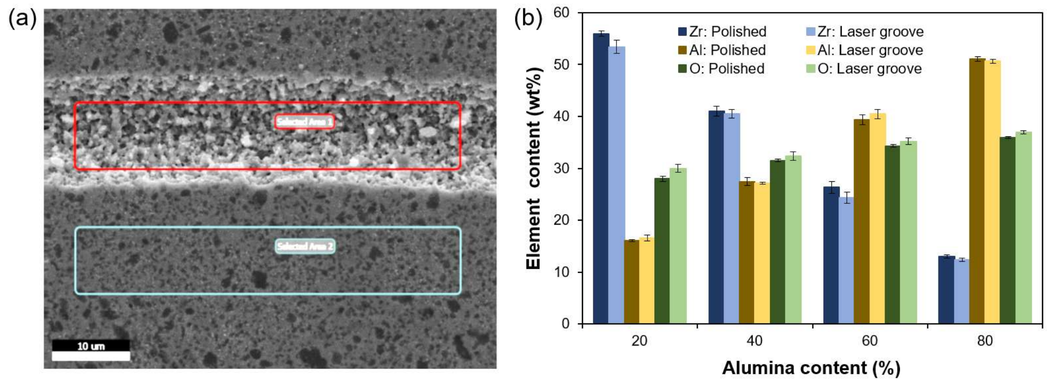

Fig. 15. (a) Representative SEM image showing the energy dispersive X-ray (EDX) measurement areas; (b) element content (wt%) of the composites of laser grooving and polished areas. The error bars represent the standard error of 5 measurements. The laser parameters for the measured grooves were: PRR of 500 kHz, scan speed of 1000 mm/s, and laser pulse energy of 6 μJ.

4. Conclusions

Femtosecond laser ablation of alumina-zirconia composite ceramics with varying alumina content from 0 to 100 wt% was performed to investigate the influence of the alumina content on the laser ablation behavior. The single pulse laser ablation thresholds as well as the incubation coefficients were determined experimentally. The influence of laser pulse energy, scan speed, and material composition on laser grooving profiles and MRR were analyzed. The conclusions are as follows:

1) The laser ablation thresholds of alumina-zirconia composites, which are ranging from 1.9 to 2.5 J/cm^2, were much smaller than those of phase pure zirconia (4.7 J/cm^2) and alumina (9.1 J/cm^2), while this difference gradually

vanished with increasing number of laser pulses under multi-pulse laser ablation conditions.

2) The composite materials were more susceptible to thermal cracks, caused by excessive heat accumulation, than the phase pure zirconia and alumina ceramics.
3) The MRR of all ceramics had nearly linear relationships with laser pulse energy. The MRR of the higher alumina content ceramics increased faster than that of lower alumina content materials with increasing laser pulse energy.
4) The scan speed had no observable influence on the MRR of the composite materials, while the MRR of zirconia and alumina decreased with increasing scan speed.
5) The composite materials showed a much larger MRR than the phase pure zirconia and alumina ceramics and this for all experimental conditions. MRR of zirconia was larger than that of alumina under low laser pulse energy conditions, while it was smaller under high laser pulse energy conditions.
6) Zirconia content of all the composites was slightly reduced after laser processing. No zirconia phase transformation was observed for 3Y-TZP and 20%-ATZ after laser processing.

This research shows that material composition will have a significant influence on the material removal behavior in femtosecond laser micromachining and highlights the need to account for this phenomena in order to optimize the machining processes.

Acknowledgements

This research was supported by Internal Funds KU Leuven through a starting grant to S.C. (STG-18-00308) and C3 IOF project (C3/20/084), and by the Research Foundation - Flanders (FWO-Vlaanderen) under grant G095920N. The authors thank Berfu Goeksel from the Department of Materials Engineering, KU Leuven, for her assistance with the micro-Raman measurements.

References

Abdo, B.M.A., El-Tamimi, A.M., Anwar, S., Umer, U., Alahmari, A.M., Ghaleb, M.A., 2018. Experimental investigation and multi-objective optimization of Nd:YAG laser micro-channeling process of zirconia dental ceramic. Int. J. Adv. Manuf. Technol. 98 (5), 2213–2230. https://doi.org/10.1007/s00170-018-2374-2.

Armbruster, O., Naghilou, A., Kautek, W., 2018. The Role of Defects in Pulsed Laser Matter Interaction. In: Advances in the Application of Lasers in Materials Science, Springer, Cham, Springer International Publishing, pp. 39–61. https://doi.org/10.1007/978-3-319-96845-2_2.

Ashkenasi, D., Lorenz, M., Stoian, R., Rosenfeld, A., 1999. Surface damage threshold and structuring of dielectrics using femtosecond laser pulses: the role of incubation. Appl. Surf. Sci. 150 (1-4), 101–106. https://doi.org/10.1016/S0169-4332(99)00228-7.

Boniecki, M., Sadowski, T., Gołębiewski, P., Węglarz, H., Piątkowska, A., Romaniec, M., Krzyżak, K., Łosiewicz, K., 2020. Mechanical properties of alumina/zirconia composites. Ceram. Int. 46 (1), 1033–1039. https://doi.org/10.1016/j.ceramint.2019.09.068.

Bonse, J., Rudolph, P., Krüger, J., Baudach, S., Kautek, W., 2000. Femtosecond pulse laser processing of TiN on silicon. Appl. Surf. Sci. 154-155, 659–663. https://doi.org/10.1016/S0169-4332(99)00481-X.

Delgado-Ruiz, R.A., Abboud, M., Romanos, G., Aguilar-Salvatierra, A., Gomez-Moreno, G., Calvo-Guirado, J.L., 2015. Peri-implant bone organization surrounding zirconia-microgrooved surfaces circularly polarized light and confocal laser scanning microscopy study. Clin. Oral Implants Res. 26 (11), 1328–1337. https://doi.org/10.1111/clr.12461.

Di Niso, F., Gaudiuso, C., Sibillano, T., Mezzapesa, F.P., Ancona, A., Lugarà, P.M., 2014. Role of heat accumulation on the incubation effect in multi-shot laser ablation of stainless steel at high repetition rates. Opt. Express 22 (10), 12200–12210. https://doi.org/10.1364/OE.22.012200.

Gautam, C., Joyner, J., Gautam, A., Rao, J., Vajtai, R., 2016. Zirconia based dental ceramics: structure, mechanical properties, biocompatibility and applications. Dalton Trans. 45 (48), 19194–19215. https://doi.org/10.1039/C6DT03484E.

Han, J., Malek, O., Vleugels, J., Braem, A., Castagne, S., 2021a. Ultrafast laser selective phase removal for surface modification of nanocomposite materials. Opt. Express 29 (16), 24834–24845. https://doi.org/10.1364/OE.433677.

Han, J., Zhang, F., Van Meerbeek, B., Vleugels, J., Braem, A., Castagne, S., 2021b. Laser surface texturing of zirconia-based ceramics for dental applications: A review. Mater. Sci. Eng., C 123, 112034. https://doi.org/10.1016/j.msec.2021.112034.

Heisterkamp, A., Herman, P.R., Meunier, M., Nolte, S., Audouard, E., Mottay, E., 2016. Engineering model for ultrafast laser microprocessing, Frontiers in Ultrafast Optics: Biomedical, Scientific, and Industrial Applications XVI., International Society for Optics and Photonics. vol. 9740, 974016. https://doi.org/10.1117/12.2206203.

Jee, Y., Becker, M.F., Walser, R.M., 1988. Laser-Induced Damage on Single-Crystal Metal-Surfaces. J. Opt. Soc. Am. B 5 (3), 648–659. https://doi.org/10.1364/JOSAB.5.000648.

Li, J., Ji, L., Hu, Y., Bao, Y., 2016. Precise micromachining of yttria-tetragonal zirconia polycrystal ceramic using 532 nm nanosecond laser. Ceram. Int. 42 (3), 4377–4385. https://doi.org/10.1016/j.ceramint.2015.11.118.

Liu, J.M., 1982. Simple technique for measurements of pulsed Gaussian-beam spot sizes. Opt. Lett. 7 (5), 196–1983. https://doi.org/10.1364/OL.7.000196.

Lu, A., Gao, Y., Jin, T., Luo, X., Zeng, Q., Shang, Z., 2020. Effects of surface roughness and texture on the bacterial adhesion on the bearing surface of bio-ceramic joint implants: An in vitro study. Ceram. Int. 46 (5), 6550–6559. https://doi.org/10.1016/j.ceramint.2019.11.139.

Lughi, V., Sergo, V., 2010. Low temperature degradation -aging- of zirconia: A critical review of the relevant aspects in dentistry. Dent. Mater. 26 (8), 807–820. https://doi.org/10.1016/j.dental.2010.04.006.

Mendelson, M.I., 1969. Average Grain Size in Polycrystalline Ceramics. J. Am. Ceram. Soc. 52 (8), 443–446. https://doi.org/10.1111/j.1151-2916.1969.tb11975.x.

Piconi, C., Maccauro, G., 1999. Zirconia as a ceramic biomaterial. Biomaterials 20 (1), 1–25. https://doi.org/10.1016/S0142-9612(98)00010-6.

Ramesh, S., Sara Lee, K.Y., Tan, C.Y., 2018. A review on the hydrothermal ageing behaviour of Y-TZP ceramics. Ceram. Int. 44 (17), 20620–20634. https://doi.org/10.1016/j.ceramint.2018.08.216.

Robertson, J., 2004. High dielectric constant oxides. EPJ Appl. Phys. 28 (3), 265–291. https://doi.org/10.1051/epjap:2004206.

Roitero, E., Lasserre, F., Anglada, M., Mucklich, F., Jimenez-Pique, E., 2017. A parametric study of laser interference surface patterning of dental zirconia: Effects of laser parameters on topography and surface quality. Dent. Mater. 33 (1), e28–e38. https://doi.org/10.1016/j.dental.2016.09.040.

Roitero, E., Ochoa, M., Anglada, M., Mücklich, F., Jiménez-Piqué, E., 2018. Low temperature degradation of laser patterned 3Y-TZP: Enhancement of resistance after thermal treatment. J. Eur. Ceram. Soc. 38 (4), 1742–1749. https://doi.org/10.1016/j.jeurceramsoc.2017.10.044.

Schunemann, F.H., Galarraga-Vinueza, M.E., Magini, R., Fredel, M., Silva, F., Souza, J.C.M., Zhang, Y., Henriques, B., 2019. Zirconia surface modifications for implant dentistry. Mater. Sci. Eng., C 98, 1294–1305. https://doi.org/10.1016/j.msec.2019.01.062.

Shugaev, M.V., Wu, C., Armbruster, O., Naghilou, A., Brouwer, N., Ivanov, D.S., Derrien, T.J.Y., Bulgakova, N.M., Kautek, W., Rethfeld, B., Zhigilei, L.V., 2016. Fundamentals of ultrafast laser–material interaction. MRS Bull. 41 (12), 960–968. https://doi.org/10.1557/mrs.2016.274.

Wei, C., Gremillard, L., 2018. Towards the prediction of hydrothermal ageing of 3Y-TZP bioceramics from processing parameters. Acta Mater. 144, 245–256. https://doi.org/10.1016/j.actamat.2017.10.061.

Figure captions:

Fig. 1. Representative SEM images of the alumina-zirconia composites after thermal etching with increasing alumina content from 0 to 100 wt% (zirconia is the bright phase, alumina is the dark one).

Fig. 2. Grain sizes of the Al_2O_3 and ZrO_2 phases in the ceramics as a function of the overall alumina content.

Fig. 3. (a) Ceramic density and relative density as a function of the alumina content; (b) Vickers hardness as a function of the alumina content.

Fig. 4. Schematic diagram of MRR determination procedure. Firstly, the average groove profile over a distance of 25 μm was extracted from the confocal microscopy measurement result. Secondly, the area of the extracted profile was calculated by the data analysis software of the confocal microscopy. The MRR can be determined by multiplying the profile area by the scan speed.

Fig. 5. (a) Squared diameter of single pulse ablation craters as a function of the logarithm of the laser fluence (J/cm^2) for the alumina-zirconia composites; (b) the single pulse ablation threshold for different materials as a function of alumina content.

Fig. 6. (a) Laser ablation thresholds under varying number of laser pulses as a function of alumina content; (b) incubation coefficients as a function of alumina content.

Fig. 7. Representative SEM images of the alumina-zirconia composites with increasing alumina content after laser ablation with (a) 1 pulse; (b) 100 pulses. The laser pulse energy was 15.4 μJ.

Fig. 8. Representative SEM images of the alumina-zirconia composites with increasing alumina content after laser grooving experiments. Laser pulse energy:15.4 μJ; scan speed: 1000 mm/s; PRR: 500 kHz.

Fig. 9. The influence of laser pulse energy on ablation groove profiles of 3Y-TZP (PRR: 500 kHz, scan speed: 1000 mm/s).

Fig. 10. (a) MRR as a function of laser pulse energy for the alumina-zirconia composites with increasing alumina contents (PRR: 500 kHz, scan speed: 1000 mm/s); (b) the slope of the fitting line in (a) as a function of alumina content.

Fig. 11. MRR as a function of scan speed for the alumina-zirconia composites with increasing alumina contents (Laser pulse energy:15.4 μJ, PRR: 500 kHz).

Fig. 12. Groove profiles of (a) 3Y-TZP and (b) 60%-Al_2O_3 under varying laser scan speeds (Laser pulse energy:15.4 μJ, PRR: 500 kHz).

Fig. 13. (a) Laser ablated groove profiles of the alumina-zirconia composites with increasing alumina content (laser pulse energy:15.4 μJ, PRR: 500 kHz, scan speed: 1000 mm/s); (b) MRR as a function of alumina content (PRR: 500 kHz, scan speed: 1000 mm/s).

Fig. 14. Micro-Raman spectra of polished and laser grooved area of 3Y-TZP and 20%-ATZ. The laser parameters for the measured grooves were: PRR of 500 kHz, scan speed of 1000 mm/s, and laser pulse energy of 6 μJ. The measurement was performed on 3 locations for each condition. One representative spectrum for each condition is shown in the figure.

Fig. 15. (a) Representative SEM image showing the energy dispersive X-ray (EDX) measurement areas; (b) element content (wt%) of the composites of laser grooving and polished areas. The error bars represent the standard error of 5 measurements. The laser parameters for the measured grooves were: PRR of 500 kHz, scan speed of 1000 mm/s, and laser pulse energy of 6 μJ.